Journal of Physics B: Atomic, Molecular and Optical Physics

PAPER

Orientation dependences of high-order harmonic generation in H_2 and H_2^+ molecules

To cite this article: V V Kim *et al* 2020 *J. Phys. B: At. Mol. Opt. Phys.* **53** 155405

IOP Publishing Journal of Physics B: Atomic, Molecular and Optical Physics

J. Phys. B: At. Mol. Opt. Phys. **53** (2020) 155405 (10pp) https://doi.org/10.1088/1361-6455/ab94c8

Orientation dependences of high-order harmonic generation in H_2 and H_2^+ molecules

V V Kim[1], R A Ganeev[1,2,3], G S Boltaev[1] and A S Alnaser[1,3]

[1] Department of Physics, American University of Sharjah, PO Box 26666, Sharjah, United Arab Emirates
[2] Faculty of Physics, Voronezh State University, Voronezh 394006, Russia

E-mail: rashid_ganeev@mail.ru and aalnaser@aus.edu

Received 21 January 2020, revised 19 April 2020
Accepted for publication 20 May 2020
Published 26 June 2020

Abstract

We propose a modified version for the strong field theory of high-order harmonic generation (HHG) in molecules and we apply it to analyze the orientation-dependences of HHG from the hydrogen molecule and it molecular ion H_2^+ when exposed to linearly polarized laser light. Our model predicts the presence of clear interference minima in the spectra of the high-order harmonics. We further exploit the orientation-dependence of the interference minima's position and the harmonics polarization properties through proposed model. We found that the position of the interference minima are associated with the polarization properties of harmonics.

Keywords: high harmonics generation, orientation dependence, strong field theory

(Some figures may appear in colour only in the online journal)

1. Introduction

High-order harmonics generation (HHG) is an example of the strong nonlinear optical response of medium at the presence of strong laser fields interacting with atoms or molecules in gaseous or plasma media, while harmonics are also generated in solids and liquids. As a source of coherent radiation at very high frequencies, this process is one of the most important aspects in strong field physics. Most of the experimental and theoretical studies of HHG have been devoted to atoms, while HHG in molecules is still a rarely-studied field, which presently leaves many open questions to address. In principle, molecules are much richer source for experimental and theoretical investigations, since their electronics level structures are more diverse and incorporating different molecular symmetries. For instance, experiments have shown that HHG spectra can be used to image molecular orbitals by calibrating the molecular re-collision electronic wave packet by a reference atom [1] and by measuring the interference minima in the HHG spectra that was predicted by numerical calculations [2–5]. Additionally, the molecular instantaneous structures have been probed during HHG [6, 7].

HHG radiation contains sufficient information about the structure of its generating medium, which allowed for orbital tomography imaging of the valence orbitals in atoms and molecules [8]. In general, the retrieval of the information about the molecular orbitals is seriously hindered by the complexity of the harmonic emission process. A commonly used experimental approach employs a pump–probe scheme, where the first pulse aligns the molecular species along its polarization direction and the second, probe pulse, after some delay, generates the high-order harmonics. The measured molecular HHG spectra are sensitive to the molecular axis orientation relative to incident laser field polarization and internuclear separation. This techniques was applied to different molecular targets, starting from simple diatomic molecules [9–11] and extending to complex polyatomic systems [12, 13]. The polarization properties of the emitted harmonics were investigated in [9, 14]. In contrast to HHG from atoms, the deviation from spherical symmetry in molecules led to observing strongly elliptically-polarized harmonics driven by linearly polarized laser fields.

[3] Author to whom any correspondence should be addressed.

Double-slit-type interference effect in the HHG spectra was theoretically predicted for the simplest diatomic molecules H_2^+ and H_2 [2, 5], and was experimentally demonstrated for aligned CO_2 molecules [6, 7]. This interference effect strongly depends of the orientation of molecular bonds with respect to the polarization direction of driving laser field and can be described as the interference between the contributions from different atoms within the molecule, which can lead to a complete suppression of some harmonics. Modification of the interference condition due to the Coulomb effects for H_2^+ was tested in [15]. Multielectron corrections in molecular HHG for different formulations of the strong-field approximation (SFA) was investigated in [16], it was found that inclusion of the multielectron corrections has very little effect on the spectrum.

Two main theoretical approaches in modelling molecules in strong laser field include direct numerical solution of time-dependent Schrödinger equations (TDSE), and theories based on the strong field approximation (SFA) [17], in which the electron motion during the time between ionization and recombination is described by the Volkov solutions of free electron in laser field. It means that its interaction with the laser field is properly treated, while the influence of the atomic or molecular binding potential is neglected. An example of such approach is the Lewenstein's model of atomic HHG [18]. Whereas direct numerical solution of the TDSE can be used for atomic and simple linear molecular targets within the single active electron (SAE) approximation, such an approach is not practical for complex molecules due to time-demanding computations. Thus, there is a need for simplified *ab initio* molecular-orbital calculations which are simple enough to be applied systematically to moderately large molecules in the presence of strong laser field.

In this work we address the problem of HHG from H_2 and H_2^+ molecules, which are very attractive for being the simplest molecular systems to test any theory. Moreover previous predictions [2, 5] on HHG from those systems have not yet been supported by experimental measurements. We present a generalized approach from [18], designated as GEX (Gaussian exact model), based on representation of initial field-free active highest occupied molecular orbital (HOMO) as linear combination of atomic orbitals (LCAO) and apply it to the problem of HHG from H_2 and H_2^+ molecules. Since, by its own ideology of SFA, all information about spatial (including all symmetries) and momentum electron distribution are contained in the initial wavefunction, it is very important to build it in a proper way. Common ways are the application of tabulated data (for example [19, 20]) of Hartree–Fock–Roothaan solutions or the determination of the coefficients by using the computational chemistry codes like GAUSSIAN [21] or GAMESS [22]. Additionally, depending on the choice, two types of basis sets appear for approximate representation of HOMO, Slater-type orbitals (STO) [23] and Gaussian-type orbitals (GTO) [24]. We chose GTO basis since it allows us to get closed analytical expression for the induced molecular dipole moment. Using the obtained expression, we analyze HHG spectra for simplest diatomic molecules H_2^+ and H_2 with various laser parameters. GTO type basis functions are widely used for molecular quantum chemical calculations. In comparison with STO, GTO type basis functions speeds up calculations by 4–5 orders of magnitude and more than outweighs the extra cost entailed by the larger number of basic functions, generally required in a Gaussian calculation, especially for large, complex molecules. Using of computational chemistry codes strongly simplifies initial step of every molecular SFA calculation.

This paper is organized as follows: the next section describes our numerical method, where analytical expressions, within the limits of the SFA model [18], for the components of induced molecular dipole momentum vector are presented, which are used to calculate HHG spectra and to determine the polarization properties of the harmonics. The third section presents the calculation results with discussion. Finally, the last section contains a short summary and our conclusions.

2. Theory

Atomic units are used throughout the paper. As a starting point of our calculations, we use the 'classical' quantum theory of HHG [18] involving the three steps: tunnel ionization from the highest occupied bounded state, acceleration of the free electron in the laser field, and recombination of the electron to the state from which it originated. The last step leads to emission of a photon. This model uses SFA and SAE. We do not take into account the contribution of intermediate resonances, ignore nuclear dynamics and consider the evolution of the molecular system only from the HOMO. Also, the decay of the active state is not taken into account, since in our calculations we restrict ourselves to laser intensities that do not give saturation of ionization for the first few optical cycles. We obtain the spectrum of HHG by calculating the Fourier transform $\mathbf{D}(\Omega)$ of the time-dependent molecular dipole moment $\mathbf{d}(t)$:

$$\mathbf{D}(\Omega) = \frac{1}{2\pi}\int_{-\infty}^{\infty} \mathrm{d}t \ \exp(i\Omega t)\mathbf{d}(t). \tag{1}$$

Instead of dipole-momentum representation alternative forms of harmonic spectra, based on the dipole velocity, and dipole acceleration can be used. It was demonstrated in [25] during numerical simulation of the hydrogen atom that for short (few-cycle) pulses or very strong (intensities $\sim 10^{15}$ W cm^{-2}) the harmonic spectra from the dipole moment are not reliable. Used in present work conditions are below this limits, also dipole momentum form was successfully applied in [26] for diatomic molecules H_2, N_2, and O_2.

Here the time-dependent induced dipole moment, with the laser field potential taken in length gauge as $-\mathbf{E}(t)\cdot\mathbf{r}$, is defined

$$\mathbf{d}(t) = 2\ \mathrm{Re}\left(i\int \mathrm{d}^3\mathbf{p}\int_0^{\infty} \mathrm{d}\tau \mathbf{E}(t-\tau)\cdot\mathbf{r}_{\mathbf{p}0}(t-\tau)\mathbf{r}_{0\mathbf{p}}(t)\right). \tag{2}$$

The amplitudes of transitions from the bound state to the continuum take the form:

$$\mathbf{r}_{\mathbf{p}0}(t) = \langle \mathbf{p} - \mathbf{A}(t)\,|\mathbf{r}|\,0\rangle \ \exp(is_{\mathrm{p}}(t) + \mathrm{i}I_{\mathrm{p}}t). \tag{3}$$

Here $\mathbf{p}$ is the electron momentum, $\mathbf{A}$(t) is the vector potential, I_{p} is the ionization potential and $s_{\mathbf{p}}(t)$ is the phase of the Volkov solution for free electron in laser field

$$s_{\mathbf{p}}(t) = \frac{1}{2}\int^{t} \mathrm{d}\tau[\mathbf{p} - \mathbf{A}(\tau)]^2. \tag{4}$$

The initial bound state is built as LCAO for the bound $1\sigma_g$ molecular orbital for H_2 molecule and H_2^+ ion and is presented as

$$\Phi_{1\sigma_g}(\mathbf{r}) = \langle \mathbf{r}|0\rangle = \sum_i b_i(\phi_i(\mathbf{r}-\mathbf{r}_0) + \phi_i(\mathbf{r}+\mathbf{r}_0)). \tag{5}$$

Here $2 \cdot r_0$ is equal to the distance between atoms in molecule. For further calculations, we generalize the approach from [18], designated as GEX model. With this approach, the basis functions $\phi_i(\mathbf{r})$ can be taken in the form of Cartesian Gaussian functions [22], forming Gaussian-type orbital (GTO) basis:

$$g_{jkl}(\xi_i, \mathbf{r}) = n(\xi_i)x^j y^k z^l e^{-\xi_i r^2} \tag{6}$$

here the normalization factor is defined as

$$n(\xi_i) = \left(\frac{2\xi_i}{\pi}\right)^{3/4}\left[\frac{(8\xi_i)^{j+k+l}\, j!k!l!}{(2j)!\,(2k)!\,(2l)!}\right]^{1/2}. \tag{7}$$

The coefficients ξ_i and b_i in (6) are obtained by Hartee–Fock calculations performed with Gaussian 03 code [21]. The STO-6G basis set [27], which approximates each basis Slater-type orbital (STO) [23] with 6 GTO's, was chosen. By itself, STO basis is widely used in simulating the interaction of bound quantum states with laser field [26] since it is consistent with the electron–nuclear cusp condition. Moreover, each orbital is constrained to have a good long-range behavior.

Developed method can be easily applied to complex molecular systems by expanding basis set. In this case additional $g_{jkl}(\xi_i,\mathbf{r})$ GTO's with defined set of ξ_i and b_i parameters will be used. H_2 and H_2^+ molecules were chosen as simplest diatomic molecular systems for examination of our approach. STO-6G basis set expressed in Gaussian-type orbitals was chosen since it allows the modeling based on STO basis. This basis set also allows comparing the results of our calculations with previous studies, for example [26], where the combination of Slater-type orbitals was used.

For the matrix element of H_2 and H_2^+ molecules in amplitude (3), we write the decomposition by g_{000} functions from the basis set (6):

$$\begin{aligned}\langle \mathbf{p}\,|r_\alpha|\,0\rangle = i\frac{\partial}{\partial p_\alpha}\tilde{\Phi}_{1\sigma_g}(\mathbf{p}) = i\sum_k \beta_k e^{-(4\xi_k)^{-1}\mathbf{p}^2} \\ \times\left\{(-(2\xi_k)^{-1}p_\alpha - ir_\alpha^{(0)})e^{-i\mathbf{p}\cdot\mathbf{r}_0} \right. \\ \left. + (-(2\xi_k)^{-1}p_\alpha + ir_\alpha^{(0)})e^{i\mathbf{p}\cdot\mathbf{r}_0}\right\}.\end{aligned} \tag{8}$$

Here the coefficients β_k include the normalization factors (7) and contraction coefficients b_k of decomposition in STO-6G basis from (5). Equation (2) can be written as:

$$\begin{aligned}d_\beta(t) = 2\ \mathrm{Re}\ i\left(\int \mathrm{d}^3\mathbf{p}\int_0^\infty \mathrm{d}\tau\left[\exp(-iS(\mathbf{p},t,\tau))\right.\right. \\ \left.\left.\times\frac{\partial}{\partial p_\beta}\tilde{\Phi}^*_{1\sigma_g}(\mathbf{p}_t)\sum_\alpha E_\alpha(t-\tau)\frac{\partial}{\partial p_\alpha}\tilde{\Phi}_{1\sigma_g}(\mathbf{p}_{t-\tau})\right]\right).\end{aligned} \tag{9}$$

The designation of the generalized momentum $\mathbf{p}_t = \mathbf{p} - \mathbf{A}(t)$ is introduced at time t and $S(\mathbf{p},t,\tau) = s_{\mathbf{p}}(t) - s_{\mathbf{p}}(t-\tau) + I_p\tau$. Subsequently, most of the works that are based on the Lewenstein's model use the Saddle point approximation for integration over momentum space, where $\mathbf{p}$ is replaced by the momentum $\mathbf{p}_{st}$ at a stationary point, which is defined by the equation:

$$\boldsymbol{p}_{st}(t,\tau) = \frac{1}{\tau}\int_{t-\tau}^{t}\mathrm{d}t'\boldsymbol{A}(t'). \tag{10}$$

It also leads to the appearance in the integrand of prefactor $(\varepsilon - i\tau/2)^{-3/2}$, with which is responsible for quantum diffusion effect and very efficiently cuts off the contributions from large τ's, which allows us to extend the integration range in (9) from 0 to infinity. The application of the generalized GEX model allows us to analytically calculate the integral over $\mathbf{p}$ in (9). We can write the result for (9) that represents the sum:

$$\begin{aligned}d_\beta(t) = 2\ \mathrm{Re}\ i\int_0^\infty \mathrm{d}\tau\left[E_\alpha(t-\tau)\left(f_{\alpha\beta}(\mathbf{r}_0,-\mathbf{r}_0)\right.\right. \\ \left.\left. + f_{\alpha\beta}(\mathbf{r}_0,\mathbf{r}_0) + f_{\alpha\beta}(-\mathbf{r}_0,-\mathbf{r}_0) + f_{\alpha\beta}(-\mathbf{r}_0,\mathbf{r}_0)\right)\right].\end{aligned} \tag{11}$$

The matrices $f_{\alpha\beta}$ with combination of arguments that correspond to contributions from the component of the dipole moment $d_\beta(t)$ for situations when ionization occurs, for example, from one atom of the molecule, and recombination on the other. This situation corresponds to the second and third terms in (11), while the ionization and recombination on the same atom correspond to the first and last terms. Omitting the intermediate transformations, we can obtain explicit representation of $f_{\alpha\beta}$ matrices:

$$\begin{aligned}f_{\alpha\beta}(\mathbf{r}_1,\mathbf{r}_2) = \sum_i\sum_j \beta_i\beta_j\left(\frac{\pi}{a_{ij}}\right)^{\frac{3}{2}} e^{0.25a_{ij}^{-1}(\mathbf{h}^{(ij)})^2 + \mathrm{F}_{ij}} \\ \times\left[\frac{B_{ij}^{(2)}\left(\{\mathbf{h}^{(ij)}\}_\alpha\{\mathbf{h}^{(ij)}\}_\beta + 2a_{ij}\delta_{\alpha\beta}\right)}{4a_{ij}^2} + \left\{\mathbf{B}_{ij}^{(0)}\right\}_{\alpha\beta}\right. \\ \left. - \frac{\left(\left\{\mathbf{B}_{ij}^{(1)}(t,\mathbf{r}_2)\right\}_\beta\{\mathbf{h}^{(ij)}\}_\alpha + \left\{\mathbf{B}_{ji}^{(1)}(t-\tau,\mathbf{r}_1)\right\}_\alpha\{\mathbf{h}^{(ij)}\}_\beta\right)}{2a_{ij}}\right].\end{aligned} \tag{12}$$

Explicit representation of the functions a_{ij}, F_{ij}, $B^{(2)}$, vectors $\mathbf{h}_{ij}$, $\mathbf{B}^{(1)}$ and matrix $\mathbf{B}^{(0)}$ in (12) are defined in the appendix . In equation (12) also appears, similar to saddle point method, the prefactor $(a_{ij})^{-3/2} = ((\xi_i^{-1} + \xi_j^{-1})/4 + i\tau/2)^{-3/2}$, which is responsible for quantum diffusion effect. Further integration by t in (1) and by τ in (11) can be also performed either numerically or using saddle point techniques. We performed integration numerically, thus accounting for the exact contributions of all saddle points and their interferences.

The coordinate system is chosen so that components of linearly polarized laser light are written in the form:

$$\mathbf{E}(t) = \{E_0\varphi(t)\cos(\omega t), 0, 0\}. \tag{13}$$

Here ω is the laser frequency, E_0 is the peak field strength, $\varphi(t)$ is equal to 1 for t from 0 to T_{pulse} (T_{pulse} is the laser pulse

duration), and 0 for the rest of the time interval. The polarization direction is fixed along x axis. The coordinates of atoms in the molecule depends on the internuclear distance $2 \cdot r_0$, the angle θ between laser polarization direction and molecular axis; and in our coordinate system have the form:

$$\begin{aligned} \mathbf{r}_1 &= \{r_0 \ \cos \ \theta, r_0 \ \sin \ \theta, 0\} \\ \mathbf{r}_2 &= \{-r_0 \ \cos \ \theta, -r_0 \ \sin \ \theta, 0\}. \end{aligned} \tag{14}$$

In our notation, d_x corresponds to the parallel component of laser polarization induced dipole moment, d_y is the nonparallel component. In the case of $\theta \neq 0$, the total spectral intensity of the N^{th} order harmonics $\Omega = N \cdot \omega$ is defined as:

$$W(\Omega) = |D_x(\Omega)|^2 + |D_y(\Omega)|^2, \tag{15}$$

where D_x and D_y are the components of Fourier transform (1). In the case of $\theta = 0^\circ$ and $\theta = 90^\circ$ only the D_x component exists and the spectral intensity is defined with $W(\Omega) = |D_x(\Omega)|^2$. The phase of α^{th} component can be written through the real and imaginary parts of D_α:

$$\varphi_\alpha(\Omega) = \arctan \frac{\text{Im } D_\alpha(\Omega)}{\text{Re } D_\alpha(\Omega)}. \tag{16}$$

For the analysis of the polarization properties of harmonics we followed the approach described in [28]. We define the Stoke's parameters for N^{th} harmonics by:

$$\begin{aligned} s_0 &= |D_x|^2 + |D_y|^2, \quad s_1 = |D_x|^2 - |D_y|^2 \\ s_2 &= 2\sqrt{|D_x|\,|D_y|}\ \cos(\varphi_y - \varphi_x), \\ s_3 &= 2\sqrt{|D_x|\,|D_y|}\ \sin(\varphi_y - \varphi_x). \end{aligned} \tag{17}$$

Using (17) we define the angle of rotation ψ of the major axes in (x, y) plane and the ellipticity ε as

$$\tan(2\psi) = s_2/s_1 \tag{18}$$

$$\varepsilon = \frac{s_3}{\sqrt{{s_1}^2 + {s_2}^2 + {s_3}^2}}. \tag{19}$$

At the same time the sign of (19) defines helicity, i.e. the direction of rotation of the polarization ellipse. The sign is positive for right-handed polarization, i.e., such that, to an observer looking in the direction from which the light is coming, the electric field vector turns in the clockwise sense.

Summarizing the content of this section, we obtained the analytical representation (within the limits of the SFA model [18]) of the induced molecular dipole moment vector using the formulas (11) and (12), the components which will be used also for calculating the polarization properties of harmonics using the relations (18) and (19).

3. Calculations and discussion

First of all, we define the initial wavefunction of the active electron at the starting moment in the absence of laser field. Figure 1 shows the probability maps $|\Phi|^2$ in the (x, y) plane for H_2 (left bottom panel) and H_2^+ (right bottom panel) molecules. These wavefunctions were obtained using the Gaussian 03 code, restricted Hartree–Fock (RHF) and unrestricted Hartree–Fock (UHF) [29] model calculations with the STO-6G basis chosen in the case of H_2 И H_2^+ molecules, respectively. The internuclear distance is fixed at $2 \cdot r_0 = 1.4$ a.u. for H_2 and $2 \cdot r_0 = 2$ a.u. for H_2^+ (figure 1, top panel). Reproduced 'vertical' ionization energy for H_2 and ionization potential for H_2^+ are close to experimental values and equal to $I_p(H_2) = 15.85$ eV (experimental value equal to 15.42 eV [30]) and $I_p(H_2^+) = 29.57$ eV (reference value 29.99 eV [31]).

Figure 2 shows the harmonics spectra calculated for H_2 neutral molecule for the laser wavelength $\lambda = 1030$ nm and laser intensity $I_n = 5 \cdot 10^{14}$ W cm^{-2}. The six panels, from (a) to (f), present the spectra at different angles θ. In panel (a) of figure 2 we plot the spectra for the limiting cases $\theta = 0^\circ$ (open red triangles) and $\theta = 90^\circ$ (filled black rhombs). In this case only D_x component of (1) exists, so the harmonics intensity is calculated as $|D_x(\Omega)|^2$. For $\theta = 90^\circ$ we obtained the Lewenstein's model-based spectrum demonstrating the well established plateau region from 60th to 150th orders with slight slope, which ends with sharp cut-off at 145th order. Cutoff position can be given quite accurate in this and the following plots by the semiempirical formula [32]

$$N_{\text{cutoff}} = \left(I_p + 3.17U_p\right)/\omega. \tag{20}$$

Here $U_p = 3.372 \cdot 10^{-7} I_n \lambda^2$ is the ponderomotive potential or quiver energy of electron. N_{cutoff}, with the parameters corresponding to figure 2, is equal to 145th order and all spectra are in a good agreement with this assessment. We did not observe any signs of intramolecular interference and it has a very clear explanation. As we can see from explicit formulas (12) and (A1)–(A6) in the case of $\theta = 90^\circ$, f_{xx} terms do not depend of r_1 and r_2 due to $\{r_1\}_x = \{r_2\}_x = 0$ and we have four equal members of sum in (11), except for two of them having independent of t exponential factor proportional to $\sim\exp(-2r_0)$, which do not contribute to the spectra. In general, the presence of exponential factor $\exp(-2r_0)$ removes the unphysical result for large internuclear distances [33] at the terms proportional to r_0 in (12).

For $\theta = 0^\circ$, when molecular axis is parallel to laser polarization direction, in panel (a) of figure 2 (open red triangles) we see the minimum in HHG spectrum located at around 117th harmonic. As one can see, this minimum has the form of valley, within which some harmonics are strongly suppressed up to 3 orders compared to the case of perpendicular orientation. The harmonics in the cutoff region are also suppressed, but the overall behavior is the same as in the previous consideration.

Panel (b) of figure 2 demonstrates the spectra for D_x (filled black circles) and D_y (open red squares) components at $\theta = 30^\circ$. Contribution for D_y becomes comparable and even bigger at the end of HHG plateau, and due to this reason the position of cutoff conforms to (20) for perpendicular component. In the spectra for D_x one can see the disappearance of minimum, which is shifted beyond the plateau region leading to the strong suppression of harmonics in the cutoff region. However, if the harmonic intensities were plotted using formula (15), one can see that the D_y component fully compensates the suppression of D_x component, so the position of cutoff will not change.

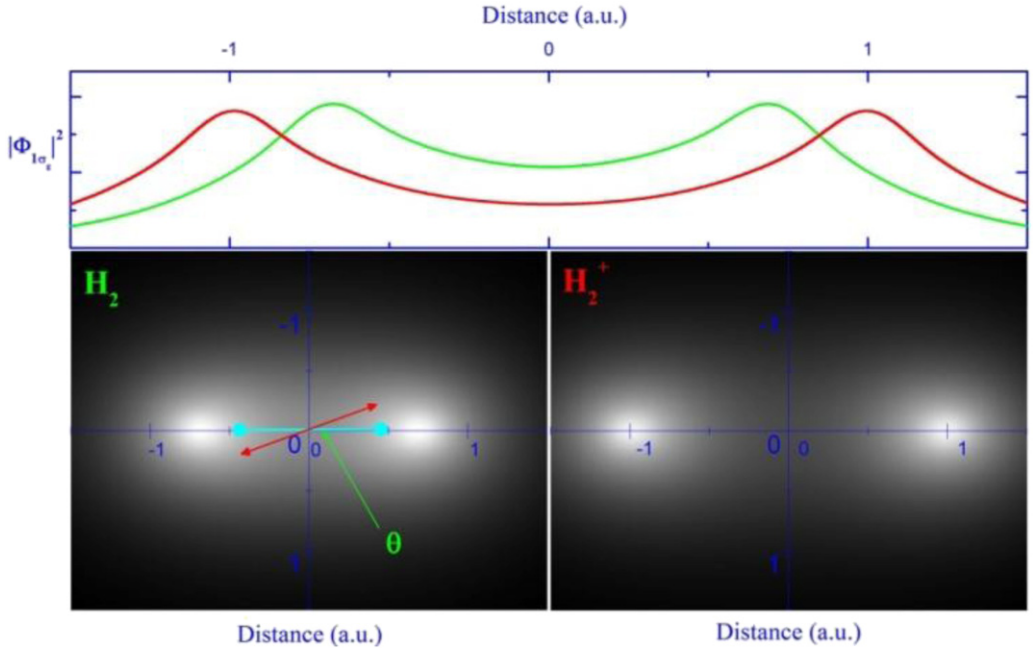

Figure 1. Probability maps for H_2 (left bottom panel) and $H_2{}^+$ (right bottom panel) molecules plotted on the base of calculation of the Gaussian 03 code [21] with schematic orientation (left bottom panel) of laser polarization axis (red arrow) and molecular axes (cyan line with 2 circles on ends). θ is the angle between these two directions. On the top panel is plotted sectional view along molecular axis for H_2 (green solid line) and $H_2{}^+$ (red solid line).

In panels (c) and (e) of figure 2 the HHG spectra are plotted for $\theta = 5^\circ$ and 15° degrees, leading to the minimum gradually shifting towards the cutoff for D_x component. In the case of panel (c), the minimum is found to be almost at the same position as for $\theta = 0^\circ$, while in the case of panel (e) its position is shifted towards the 125th order. The contribution from D_y component (open red squares) increases with angle θ and in the case of panels (e) and (b) exceeds the component parallel to laser field polarization. The calculations of the harmonics intensity W using equation (15) lead to disappearance of the minimum in HHG spectra, as one can see this in (d) and (f) panels (filled blue triangles). Overall the picture shows well expressed minima only for the angles close to $\theta = 0^\circ$. The disappearance of interference minimum in the total HHG spectra for large alignment angles was predicted previously in [4] for $H_2{}^+$ by the 3D TDSE method, so we confirm same effect for H_2 molecule.

The nonzero contribution from D_y component allows us to expect strong changes in the polarization properties of the HHG emission. It can result in the rotation of polarization direction for harmonics and even the generation of elliptically polarized harmonics depending on the phases φ_x and φ_y (16). The calculated ellipticities (19) for $\theta = 5^\circ$ and 15° are presented as insets in panels (d) and (f). The red solid circles correspond to ellipticity for orientation at positive directions $\theta = +5^\circ$ and $+15^\circ$ of the molecular axis relative to laser polarization direction. The green solid circles are the same for negative angles $\theta = -5^\circ$ and -15°.

For the group of harmonics at around the minima we observe strong changes in the polarization properties when the ellipticity reaches the values close to 1 corresponding to circularly polarized light. Also it is demonstrated that the helicity of harmonics can be controlled by changing the orientation of molecular axis, when the direction of rotation of polarized harmonics corresponds to the sign of angle θ. The experimental polarimetry measurements of high-order harmonic emission from aligned molecules of N_2 were reported in [14]. They found that the elliptically polarized harmonics can be emitted by N_2 driven by linearly polarized laser field and that the phase difference between the D_x and D_y components of the HHG strongly depends on the harmonic order. We cannot directly compare this experiment with our calculations since N_2 molecule requires further consideration within the approach presented in our research. However, it is clear that the interference minima may be associated with strong variations of the polarization properties of harmonics and vice verse.

The two-centre interference and the influence of the coulombic potential on the polarization direction and ellipticity was discussed in [34] by 2D TDSE for $H_2{}^+$ ion. Authors of [34] observed significant ellipticity of the emitted harmonics around the interference minimum and this result was attributed with Coulomb effects. Main difference of our results from [34] that in the plane-wave approximation for the returning electron was not expected to see any ellipticity, but this is what demonstrated in present work.

In order to demonstrate the movement of interference minima for larger angles one has to increase the length of plateau region, and one way to do that is by increasing the laser intensity. Another way would be by choosing a laser with longer wavelength, since N_{cutoff} in (20) is proportional to λ^2. Therefore, by increasing the fundamental laser wavelength we can extend the harmonic cutoff to higher orders whilst keeping the laser parameters below the saturation intensity. This approach was adopted to expand the technique of HHG spectroscopy

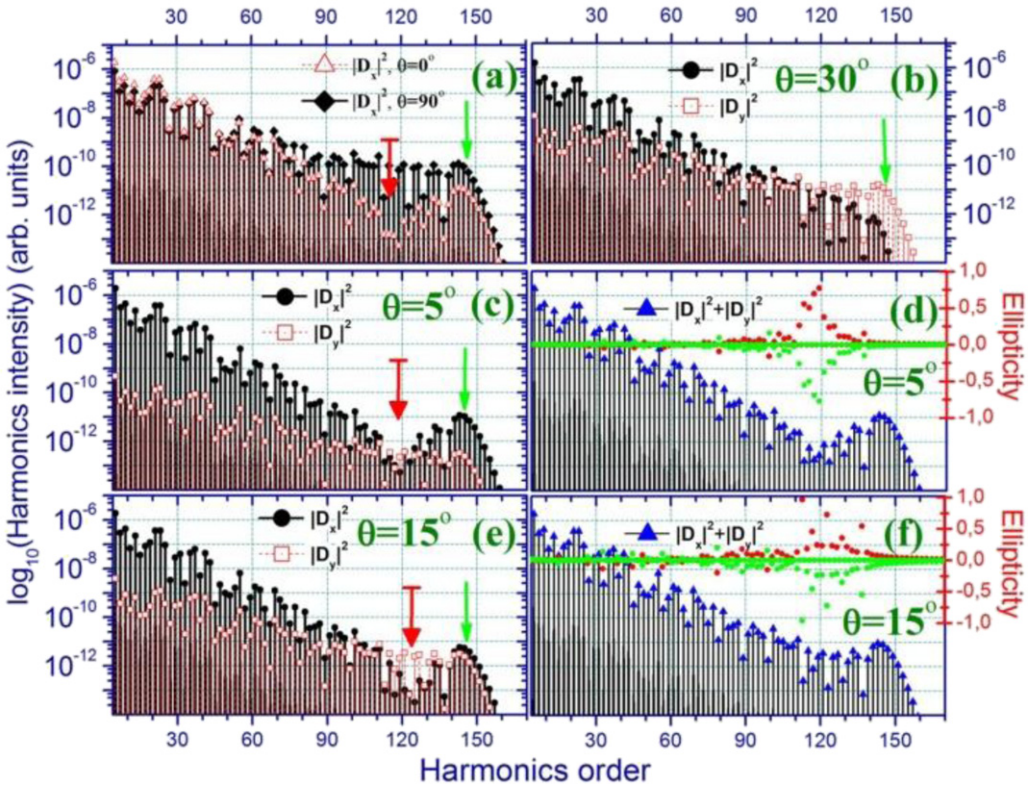

Figure 2. Calculated harmonic spectra for H_2 molecule with $\lambda = 1030$ nm, $I_n = 5 \cdot 10^{14}$ W cm^{-2}. Red arrows show the positions of minima and green arrows show the positions of cutoff. Panel (a) presents HHG spectra for D_x component of (1) at $\theta = 0^\circ$ (red open triangles) and $\theta = 90^\circ$ (black filled circles). Panel (b) shows the spectra for D_x (filled black circles) and D_y (open red squares) components at $\theta = 30^\circ$. Panel (c) shows the spectra for D_x (filled black circles) and D_y (open red squares) at $\theta = 5^\circ$. Panel (d) shows the harmonics spectral intensity W (15) (filled blue triangles) at $\theta = 5^\circ$; inset presents the calculated ellipticity (19) for $\theta = +5^\circ$ (solid red circles) and $\theta = -5^\circ$ (green solid circles). Panel (e) shows the spectra for D_x (filled black circles) and D_y (open red squares) at $\theta = 15^\circ$. Panel (f) shows the harmonic spectral intensity W (filled blue triangles) at $\theta = 15^\circ$; inset presents the calculated ellipticity for $\theta = +15^\circ$ (solid red circles) and $\theta = -15^\circ$ (green solid circles).

in [13] by using the 1300 nm laser wavelength. However, a consequence of increasing the wavelength is that the laser cycle and hence the time the electron spends in the continuum between ionization and recombination increases in proportion to λ, which results in a reducing the probability of recollision [18]. Additionally, the harmonic yield scales with the laser wavelength as λ^{-5} or λ^{-6} [35–37]. Hence, a balance between extending the cutoff and losing harmonic efficiency must be found.

In figure 3 we plot the results for $\lambda = 1300$ nm and $I_n = 5 \cdot 10^{14}$ W cm^{-2}. At these parameters of laser field we have $N_{\text{cutoff}} = 281$ (20). Panel (a) of figure 3, similar to panel (a) of figure 2, shows the spectra for the limiting cases $\theta = 0^\circ$ (open red triangles) and $\theta = 90^\circ$ (filled black rhombuses). Here we observe a well determined minima in the plateau at around the 145th harmonic for D_x at $\theta = 0^\circ$. Since the minimum is placed deep inside the plateau, its valley does not affect the cutoff region. The interference minima travel at $\theta = 15^\circ$, 30° and 45° (panels (b), (c) and (d)) for the D_x component parallel to laser field (open red square), with the positions of minima corresponding to 155th, 189th, and 269th orders. For panels (b), (c) and (d) the total spectral intensity W (15) (black filled circles) was calculated since the existence of the non-zero contribution of D_y. One can again see that with increasing θ the effect of minima vanishes. This feature is clearly seen on panels (c) and (d) where we have the flat plateau region for W (15). As a result, it will be impossible to recognize the presence of minima at high θ in the experiments with harmonics detectors based on intensity or photons counting techniques. Another conclusion is a requirement of very accurate orientation of molecules in space by prepulse, since the interference minima is well observed only for narrow angles at around $\theta = 0^\circ$ as well as dependence of interference minima position on the molecular angle can shift its position beyond plateau region.

Concerning polarization properties, our model predicts the existence of elliptically polarized harmonics at around the spectral minima at small values of θ. This peculiarity is demonstrated in panel (b) of figure 3. The ellipticity of harmonics (19) are plotted with solid red and green circles, corresponding to the rotation of molecular axis in positive ($\theta = +15^\circ$) and negative ($\theta = -15^\circ$) directions. Panels (c) and (d) of figure 3 show that, with increasing angle θ, the ellipticity decreases. However, since the D_y compensates a decrease of D_x in the region of minima, the polarization direction of harmonics becomes oriented along y direction, thus remaining linearly polarized. This effect strongly expressed for cutoff harmonics at $\theta = 45^\circ$ in panel (d) of figure 3.

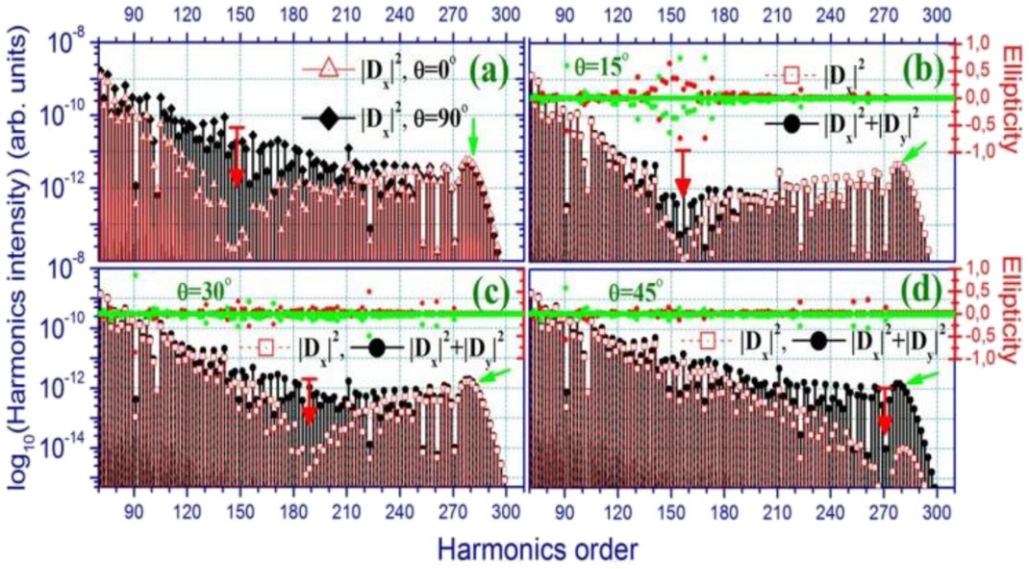

Figure 3. Calculated harmonic spectra for H_2 molecule with $\lambda = 1300$ nm and $I_n = 5 \cdot 10^{14}$ W cm^{-2}. Red arrows show the positions of the minima and green arrows indicate the cutoffs. Panel (a) presents the HHG spectra for D_x component of (1) at $\theta = 0°$ (red open triangles) and $\theta = 90°$ (black filled rhombus). Panel (b) shows the spectra for D_x component (open red squares) and W (15) (filled black circles) at $\theta = 15°$; inset presents the calculated ellipticity (19) for $\theta = +15°$ (solid red circles) and $\theta = -15°$ (solid green circles). Panel (c) shows the spectra for D_x component (open red squares) and W (filled black circles) at $\theta = 30°$; inset presents the ellipticities for $\theta = +30°$ (solid red circles) and $\theta = -30°$ (green solid circles). Panel (d) shows the spectra for D_x component (open red squares) and W (filled black circles) at $\theta = 45°$; inset presents the ellipticities for $\theta = +45°$ (solid red circles) and $\theta = -45°$ (green solid circles).

Our model calculations of H_2 molecule show that position of interference minimum is completely independent of the wavelength and intensity of laser field. In figure 4, panel (a) we plot the HHG spectra with three different sets of laser parameters for parallel orientation ($\theta = 0°$) of molecular and polarization axes. The first set is for $\lambda = 800$ nm, $I_n = 8 \cdot 10^{14}$ W cm^{-2} (black filled squares). Here we ignore the problem of ground state depletion. This intensity was chosen to extend the plateau region. The second set is for $\lambda = 1030$ nm, $I_n = 5 \cdot 10^{14}$ W cm^{-2} (filled red triangles) and the third set is for $\lambda = 1300$ nm, $I_n = 3 \cdot 10^{14}$ W cm^{-2} (blue filled circles). All three spectra in case $\theta = 0°$ have the minima at $\lambda_H = 8.7$ nm, which corresponds to the 91th, 117th and 147th harmonics for each given laser wavelengths. Panel (b) of figure 4 shows the spectra for D_x component at $\theta = 30°$ for $\lambda = 1030$ nm, $I_n = 7 \cdot 10^{14}$ W cm^{-2} (filled red squares) and $\lambda = 1300$ nm, $I_n = 5 \cdot 10^{14}$ W cm^{-2} (filled blue squares). The position of minima in case $\theta = 30°$ is shifted to $\lambda_H = 6.8$ nm, which corresponds to the 151th and 191th harmonics.

We also performed the calculation for H_2^+ ion in order to define the dependence of HHG on the internuclear distance using the 'real' model. The equilibrium distance in this ion is equal to 2 a.u., which is larger compared to H_2 molecule. The ionization potential is also increased up to 30 eV, which will lead to the extension of HHG plateau length.

In our model calculations for H_2^+ based on the SFA approach and building of approximated wavefunction as LCAO in the same STO-6G basis as for H_2 molecule, the difference between these two molecules is encapsulated in increased ionization energy (29.57 eV vs 15.85 eV), increased internuclear distance (2 a.u. vs 1.4 a.u.) and another set of b_i coefficients in (5). Increasing of ionization potential leads

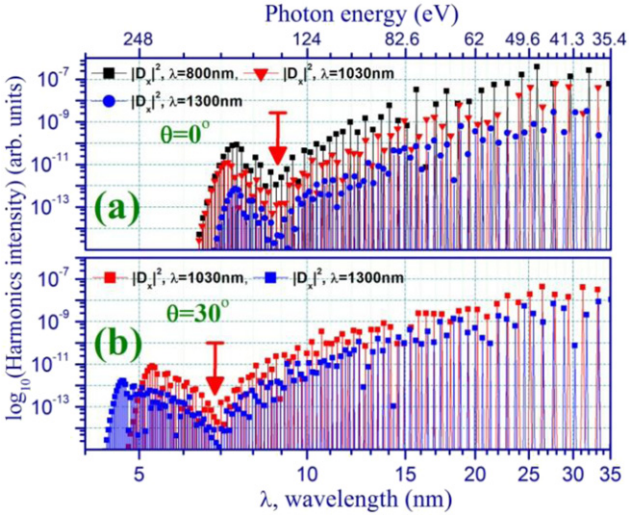

Figure 4. Calculated harmonic spectra for H_2 molecule. Red arrows show the position of interference minima. Panel (a) shows the HHG spectra for D_x component of (1) at $\theta = 0°$ using $\lambda = 800$ nm, $I_n = 8 \cdot 10^{14}$ W cm^{-2} (filled black squares), $\lambda = 1030$ nm, $I_n = 5 \cdot 10^{14}$ W cm^{-2} (filled red triangles) and $\lambda = 1300$ nm, $I_n = 3 \cdot 10^{14}$ W cm^{-2} (filled blue circles). Panel (b) shows the HHG spectra for D_x component of (1) at $\theta = 30°$ using $\lambda = 1030$ nm, $I_n = 7 \cdot 10^{14}$ W cm^{-2} (filled red squares) and with $\lambda = 1300$ nm, $I_n = 5 \cdot 10^{14}$ W cm^{-2} (filled blue squares).

to increasing cutoff order and decreasing harmonics signal. However, the shift of interference minima in HHG spectra may be associated exclusively with increasing internuclear distance.

In figure 5 we present the calculated HHG spectra from H_2^+ ion at different laser parameters and θ. Panel (a) of figure 5

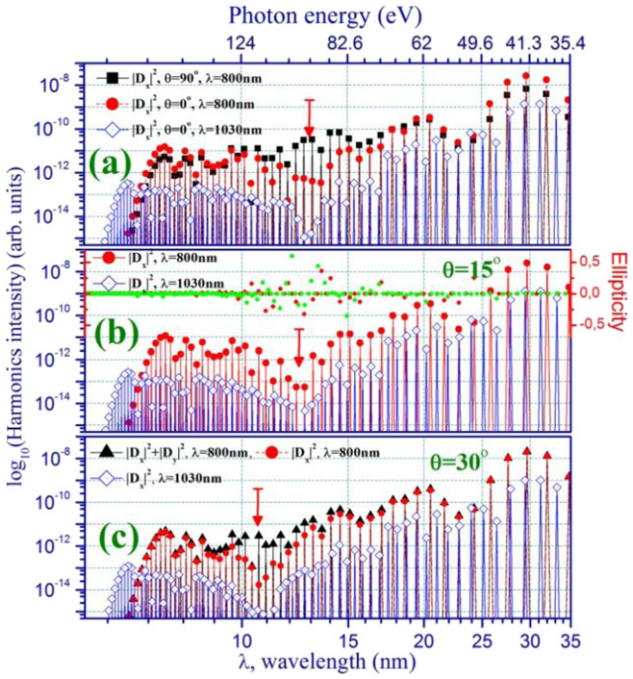

Figure 5. Calculated harmonic spectra for H_2^+ ion. Red arrows show the positions of interference minima. Panel (a) shows the HHG spectra for D_x component of (1) at $\theta = 0°$, with $\lambda = 800$ nm, $I_n = 7 \cdot 10^{14}$ W cm^{-2} (filled red circles), at $\theta = 90°$, with $\lambda = 800$ nm, $I_n = 7 \cdot 10^{14}$ W cm^{-2} (filled black squares), and at $\theta = 90°$ with $\lambda = 1030$ nm, $I_n = 5 \cdot 10^{14}$ W cm^{-2} (open blue rhombuses). Panel (b) shows the HHG spectra for D_x component at $\theta = 15°$, with $\lambda = 800$ nm, $I_n = 7 \cdot 10^{14}$ W cm^{-2} (filled red circles) and with $\lambda = 1030$ nm, $I_n = 5 \cdot 10^{14}$ W cm^{-2} (open blue rhombuses). Inset shows the ellipticity of harmonics for $\lambda = 800$ nm (solid red circles) and $\lambda = 1030$ nm (green solid circles). Panel (c) shows the HHG spectra for D_x component at $\theta = 30°$, with $\lambda = 800$ nm, $I_n = 7 \cdot 10^{14}$ W cm^{-2} (filled red circles) and with $\lambda = 1030$ nm, $I_n = 5 \cdot 10^{14}$ W cm^{-2} (open blue rhombuses), and total harmonic yield W (15) at $\theta = 30°$, with $\lambda = 800$ nm, $I_n = 7 \cdot 10^{14}$ W cm^{-2} (filled black triangles).

shows the HHG spectra at $\theta = 0°$ (filled red circles) and $\theta = 90°$ (filled black squares) of D_x component (1) for $\lambda = 800$ nm, $I_n = 7 \cdot 10^{14}$ W cm^{-2} and at $\theta = 0°$ (open blue rhombs) for $\lambda = 1030$ nm, $I_n = 5 \cdot 10^{14}$ W cm^{-2}. N_{cutoff} is equal to $\lambda_{800nm} = 7.6$ nm (105-th order) and $\lambda_{1030nm} = 6.56$ nm (157th order) for the correspondent wavelengths of the driving pulses. HHG spectra at $\lambda = 800$ nm are combined for $\theta = 0°$ and $\theta = 90°$, since the interference minimum in the former case is not so pronounced and it is simpler to recognize it with regard to the background spectrum at $\theta = 90°$. The positions of minima for these wavelengths are at around $\lambda_H = 13$ nm (61th and 79th orders). Panels (b) and (c) show the positions of minima for $\theta = 15°$ and 30°. One can see that, for small angles (0° and 13°), the positions of minima almost coincide with each other. Inset in panel (b) demonstrates the polarization properties of emitted harmonics for $\lambda = 800$ nm (solid red circles) and $\lambda = 1030$ nm (solid green circles). Group of harmonics at around minima are elliptically polarized, similarly to the cases shown in figures 2 and 3. Panel (c) shows the total intensity W (15) at $\lambda = 800$ nm (black filled triangles) where the minimum was suppressed, since the D_y component becomes dominant. As a result, similar to the one described in the case of the panel (c) of figure 3, the ellipticity decreases and harmonics become mainly polarized in the y axis direction. The position of minima for $\theta = 30°$ is at $\lambda_H = 10.6$ nm, which corresponds to the 75th order of $\lambda = 800$ nm and 97th order of $\lambda = 1030$ nm.

The comparison of minima positions shows a shift at $\theta = 0°$ from $\lambda_0(H_2) = 8.7$ nm for H_2 to $\lambda_0(H_2^+) = 13$ nm for H_2^+. Similar comparisons show the shifts at $\theta = 30°$ from $\lambda_{30}(H_2) = 6.8$ nm to $\lambda_{30}(H_2^+) = 10.6$ nm and at $\theta = 45°$ from $\lambda_{45}(H_2) = 4.8$ nm to $\lambda_{45}(H_2^+) = 8.1$ nm. It was suggested in [3] that the positions of the interference extrema are approximately reproduced by suggesting an analogy to the interference between the two point sources. The double-slit-type or two-point emitter interference in HHG manifests as minima and maxima in the harmonic yield. These two-centre interference minima and maxima, respectively, are expected for:

$$2r_0 \cos\theta = (2n+1)\frac{\lambda_k}{2}, \qquad 2r_0 \cos\theta = n\lambda_k, \quad (n = 0, 1, 2, \ldots). \tag{21}$$

Here $\lambda_k = 2\pi/k$ is the de Broglie wavelength of the electron having kinetic energy $k^2/2 = (2N + 1)\omega$ equal to the emitted high-harmonic photon energy.

This simple model was supported by the numerical results for H_2^+ and H_2 [2, 3, 5]. We would like to highlight the results of [26], where various versions of SFA in length gauge with or without the dressing of the initial and/or final molecular state was investigated. It was previously shown [26] that clear two-centre interference minima in the harmonic spectra as a function of the molecular orientation appear only if the final molecular state is undressed. The best expressed minima correspond to undressed initial state and undressed final molecular state version of SFA and in the case of H_2 molecule are well described by (21). According to (21), the first minima ($n = 0$) of harmonics for angles $\theta = 0°$, 30° and 45° are equal to $\lambda_0(H_2) = 18$ nm, $\lambda_{30}(H_2) = 13.5$ nm and $\lambda_{45}(H_2) = 9$ nm for H_2, $\lambda_0(H_2^+) = 36.9$ nm, $\lambda_{30}(H_2^+) = 27.6$ nm and $\lambda_{45}(H_2^+) = 18.4$ nm for H_2^+, while demonstrating the scaling as $(2r_0 \cos(\theta))^2$. In comparison, our calculations show the shift of interference minima positions towards the short-wavelength region, while their positions are scaling with $a(r_0) - b(r_0)\sin^2(\theta)$ dependence.

Figure 6 shows the summary dependences of the positions of minima on the angle θ in the cases of the simulated positions for H_2 (red crossed circles) and H_2^+ (black crossed squares), fitting by $a(r_0) - b(r_0)\sin^2(\theta)$ dependence (solid red and black lines, correspondingly) and predictions derived from (21) (dashed red and black lines). We found a contradiction of ours results compared with those from [26], as with works based on direct numerical calculations based on TDSE [2, 3, 5]. This is the most contradicting result of our model, since our scaling law presents alternative to those presented in other works. At this moment, we do not have clear explanation on this contradiction. At the same time we did not have problems with other results, like cut-off [it is perfectly described by $(I_p + 3.17U_p)/\omega$ rule, without predicted deviations in the case of using length-gauge for bigger intramolecular distance (H_2 to

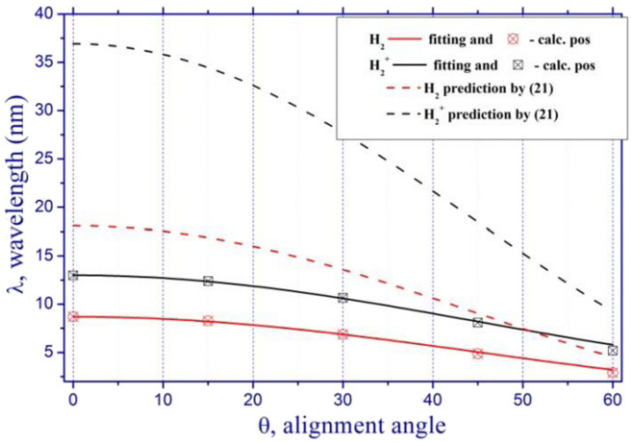

Figure 6. Comparison of the interference minima of harmonic wavelength position for D_x component of (1) calculated for H_2 (red crossed circles) and H_2^+ (black crossed squares). Solid red and black lines are the fittings based on the $a(r_0) - b(r_0)\sin^2(\theta)$ relation. Dashed red and black lines are the predictions determined from the formula (21).

H_2^+)], presence of interference minima, it is dependence only of molecular parameters, predictable polarization properties, and so on.

We also would like to mention the study [38], where authors in the same manner investigated the orientation dependence of HHG from H_2^+ and theirs numerical simulations by direct solving of TDSE in length gauge and using similar to [26] SFA model demonstrated that at certain harmonic orders the envelopes of the HHG spectra taken at different orientation angles intersect and the position of intersection is largely independent of the laser intensity while strongly dependent on the internuclear distance. This striking 'intersection' phenomenon was identified as due to intramolecular two-centre interference in the HHG. Similar conditions were used in [38] as those shown in figure 5, but they did not obtain clear interference minima. Our model ideologically is close to undressed–undressed version of [26], even we used different basis set (GTO) instead of STO used in [26]. However, we have chosen the STO-6G basis set approximating each Slater-type orbital with 6 GTO's by least-squares methods, which for small sized molecules gives very similar results in computing the initial ground state wavefunctions. The significant difference is the use by authors of [26] the Saddle point approximations for evaluating all integrals in (1) and (9). The results of [26] achieved a good agreement with the numerical calculations [2, 3, 5] concerning position of interference minima, but ours are not agree and present alternative behavior. However, as final remark we would like to note that to date the interference effect has not been observed experimentally in H_2 and further researches are required.

4. Conclusions

In conclusion, we have studied the HHG from the molecular systems H_2 and H_2^+, with simplest structure in frame of modified version of SFA theory [18]. Generalization of GEX model [18], combined with LCAO representation of HOMO allowed us to analytically calculate the three-dimensional integrals over **p** in (9), without using Saddle-point technique. We have demonstrated the explicit influence of HOMO symmetry on such a peculiarity of HHG spectra, as the presence of interference minima. We confirmed the conclusions of the numerical simulations on the base of direct TDSE solution [2, 3, 5] that the position of interference minima in HHG spectra does not depend on the parameters of laser radiation, such as wavelength and intensity. The position of minima strongly depends only on the internuclear distance in molecule for bonding molecular orbital and angle θ between the polarization direction of linearly polarized laser field and the molecular axis. In comparison with [26] our calculations gave the strong shift of interference minima positions to the short-wavelength region and the alternative scaling law with $\sin^2(\theta)$ dependence. We have demonstrated that the polarization properties of harmonics at around the minima region are strongly change with variation of θ. Depending on the position of minimum regarding to the cutoff region and angle θ, the linearly polarized, but aligned in perpendicular to the driving laser polarization harmonics, as well as the elliptically and even circularly polarized harmonics appear. Finally, our model calculations predict the vanishing of minima effect in HHG spectra in the case if one takes in to account the D_y component of harmonics. For the spectral intensity calculated as $|D_x|^2 + |D_y|^2$ with increasing of angle θ the interference minimum may be indistinguishable in experiments where harmonic detectors are based on intensity or photons counting technique.

Appendix

In this section we present the explicit representation of the functions a_{ij}, F_{ij}, $B^{(2)}$, vectors $\mathbf{h}_{ij}$, $\mathbf{B}^{(1)}$ and matrix $\mathbf{B}^{(0)}$:

$$a_{ij} = (\xi_i^{-1} + \xi_j^{-1})/4 + i\tau/2 \tag{A1}$$

$$\mathbf{h}_{ij}(\mathbf{r}_1, \mathbf{r}_2) = -0.5(\xi_i^{-1}\mathbf{A}(t-\tau) + \xi_j^{-1}\mathbf{A}(t)) + i\left(\mathbf{r}_1 + \mathbf{r}_2 - \int_{t-\tau}^{t} \mathrm{d}t'\mathbf{A}(t')\right) \tag{A2}$$

$$\mathrm{F}_{ij}(\mathbf{r}_1, \mathbf{r}_2) = -\frac{1}{4}(\xi_i^{-1}\mathbf{A}^2(t-\tau) + \xi_j^{-1}\mathbf{A}^2(t)) + i(\mathbf{A}(t-\tau)\cdot\mathbf{r}_1 + \mathbf{A}(t)\cdot\mathbf{r}_2 - \frac{1}{2}\int_{t-\tau}^{t} \mathrm{d}t'\mathbf{A}^2(t') - I_\mathrm{p}\tau) \tag{A3}$$

$$\mathrm{B}_{ij}^{(2)} = 0.25(\xi_i\xi_j)^{-1} \tag{A4}$$

$$\mathbf{B}_{ij}^{(1)}(t, \mathbf{r}) = -0.25(\xi_i\xi_j)^{-1}\mathbf{A}(t) + 0.5i\xi_i^{-1}\mathbf{r} \tag{A5}$$

$$\left\{\mathbf{B}_{ij}^{(0)}(\mathbf{r}_1, \mathbf{r}_2)\right\}_{\alpha\beta} = \frac{A_\alpha(t-\tau)A_\beta(t)}{4\xi_i\xi_j} - \{\mathbf{r}_1\}_\alpha\{\mathbf{r}_2\}_\beta - 0.5i\left(\xi_i^{-1}A_\alpha(t-\tau)\{\mathbf{r}_2\}_\beta + \xi_j^{-1}A_\beta(t)\{\mathbf{r}_1\}_\alpha\right). \tag{A6}$$

The coefficients of STO-6G basis set can be found in [39].

Acknowledgments

These studies were supported by FRG AS1801 grant and the Common Research Facility at the American University of Sharjah.

ORCID iDs

R A Ganeev https://orcid.org/0000-0001-5522-1802
A S Alnaser https://orcid.org/0000-0003-4822-9747

References

[1] Itatani J, Levesque J, Zeidler D, Niikura H, Pepin H, Kieffer J C, Corkum P B and Villeneuve D M 2004 *Nature* **432** 867
[2] Lein M, Hay N, Velotta R, Marangos J P and Knight P L 2002 *Phys. Rev. Lett.* **88** 183903
[3] Lein M, Hay N, Velotta R, Marangos J P and Knight P L 2002 *Phys. Rev.* A **66** 023805
[4] Lein M, Corso P P, Marangos J P and Knight P L 2003 *Phys. Rev.* A **67** 023819
[5] Kamta G L and Bandrauk A D 2005 *Phys. Rev.* A **71** 053407
[6] Kanai T, Minemoto S and Sakai H 2005 *Nature* **435** 470
[7] Vozzi C *et al* 2005 *Phys. Rev. Lett.* **95** 153902
[8] Vozzi C, Negro M, Calegari F, Sansone G, Nisoli M, De Silvestri S and Stagira S 2011 *Nat. Phys.* **7** 822
[9] Mairesse Y, Levesque J, Dudovich N, Corkum P B and Villeneuve D M 2008 *J. Mod. Opt.* **55** 2591
[10] Levesque J, Mairesse Y, Dudovich N, Pépin H, Kieffer J-C, Corkum P B and Villeneuve D M 2007 *Phys. Rev. Lett.* **99** 243001
[11] Velotta R, Hay N, Mason M B, Castillejo M and Marangos J P 2001 *Phys. Rev. Lett.* **87** 183901
[12] Kraus P M *et al* 2015 *Nat. Commun.* **6** 7039
[13] Torres R *et al* 2010 *Opt. Express* **18** 3174
[14] Zhou X, Lock R, Wagner N, Li W, Kapteyn H C and Murnane M M 2009 *Phys. Rev. Lett.* **102** 073902
[15] Ciappina M F, Chirilă C C and Lein M 2007 *Phys. Rev.* A **75** 043405
[16] Augstein B B and Figueira de Morisson Faria C 2011 *J. Mod. Opt.* **58** 1173–87
[17] Keldysh L V 1964 *Zh. Eksp. Teor. Fiz.* **47** 1945
Keldysh L V 1965 *Sov. Phys. - JETP* **20** 1307
[18] Lewenstein M, Balcou P, Ivanov M Y, L'Huillier A and Corkum P B 1994 *Phys. Rev.* A **49** 2117
[19] Cade P E, Sales K D and Wahl A C 1966 *J. Chem. Phys.* **44** 1973
[20] Cade P E and Wahl A C 1974 *At. Data Nucl. Data Tables* **13** 339
[21] Frisch M J *et al* 2003 *Gaussian 03, Revision A.1* (Pittsburgh, PA: Gaussian, Inc.)
[22] Schmidt M W *et al* 1993 *J. Comput. Chem.* **14** 1347
[23] Slater J C 1930 *Phys. Rev.* **36** 57
[24] Boys S F 1950 *Proc. R. Soc. Lond. A.* **200** 542
[25] Bandrauk A D, Chelkowski S, Diestler D J, Manz J and Yuan K-J 2009 *Phys. Rev.* A **79** 023403
[26] Odžak S and Milošević D B 2009 *Phys. Rev.* A **79** 023414
[27] Hehre W J, Stewart R F and Pople J A 1969 *J. Chem. Phys.* **51** 2657
[28] Antoine P, L'Huillier A, Lewenstein M, Salières P and Carrè B 1996 *Phys. Rev.* A **53** 1725
[29] Roothan C C J 1951 *Rev. Mod. Phys.* **23** 69
Pople J A and Nesbet R K 1954 *J. Chem. Phys.* **22** 571
McWeeny R and Dierksen G 1968 *J. Chem. Phys.* **49** 4852
[30] McCormack E, Gilligan J M, Cornaggia C and Eyler E E 1989 *Phys. Rev.* A **39** 2260
[31] Tong X M, Zhao Z X and Lin C D 2002 *Phys. Rev.* A **66** 033402
[32] Krause J L, Schafer K J and Kulander K C 1992 *Phys. Rev. Lett.* **68** 3535
[33] Milošević D B 2006 *Phys. Rev.* A **74** 063404
[34] Zwan E V and Lein M 2010 *Phys. Rev.* A **82** 033405
[35] Shan B and Chang Z 2001 *Phys. Rev.* A **65** 011804
[36] Tate J, Auguste T, Muller H G, Salières P, Agostini P and DiMauro L F 2007 *Phys. Rev. Lett.* **98** 013901
[37] Shiner A D *et al* 2009 *Phys. Rev. Lett.* **103** 073902
[38] Chen Y J, Liu J and Hu B 2009 *J. Chem. Phys.* **130** 044311
[39] Benjamin P P, Doaa A, Brett D, Tara D G and Theresa L W 2019 *J. Chem. Inf. Model.* **59** 4814–20